

F30: CCD photometry in modern astronomy

carried out by

Mathieu Kaltschmidt and Quirinus Schwarzenböck

on August 27th / 28th 2018

at

Max-Planck-Institut für Astronomie

Königstuhl 17
69117 Heidelberg

Supervisor: Asmita Bhandare

handed in as special report on: *November 14, 2018*

Graded: _____

Date, Signature

F30: CCD photometry in modern astronomy

Mathieu Kaltschmidt and Quirinus Schwarzenböck

Abstract

This experiment has been performed as part of the advanced lab course for physics students (FP) at Heidelberg University.

The theoretical and experimental basic knowledge which is needed for the understanding of the conducted measurements is introduced and important concepts of modern astronomical research are presented and discussed.

The characteristics of a CCD-camera are analyzed using data we recorded with the KING telescope at MPIA.

Furthermore important astronomical data analysis tools used in current research are introduced and applied to our measurements.

Lastly we use an image of the globular cluster BS90¹⁴ taken by the Hubble Space Telescope (HST) to generate a Color-Magnitude Diagram in order to determine age and metallicity of the cluster.

Zusammenfassung

Dieses Experiment wurde im Rahmen des Fortgeschrittenen-Praktikums für Studierende der Physik (FP) an der Universität Heidelberg durchgeführt.

Es werden die theoretischen und experimentellen Grundlagen zum Verständnis der durchgeführten Messungen vorgestellt und grundlegende Konzepte moderner astronomischer Forschung erläutert und diskutiert.

Die charakteristischen Eigenschaften einer CCD-Kamera werden am Beispiel unserer Messungen mit dem KING-Teleskop am MPIA überprüft und wichtige Elemente der astronomischen Datenanalyse eingeführt.

Am Beispiel einer Aufnahme des Kugelsternhaufens BS90¹⁴, welche vom Hubble Space Telescope (HST) aufgezeichnet wurde wird ein Farben-Helligkeits-Diagramm erstellt und damit das Alter und die Metallizität des Sternhaufens ermittelt.

Contents

1	Fundamental principles of astronomical measurements	1
1.1	Detectors in Astronomy	1
1.2	Data Reduction	2
1.3	Basics of photometry	2
1.4	Magnitudes	3
1.4.1	Instrumental Magnitude	3
1.4.2	Apparent Magnitude	4
1.4.3	Absolute Magnitude	4
1.5	Bolometric Magnitude	5
1.6	The Hertzsprung-Russel-Diagram	6
1.6.1	Analysis of a Color Magnitude Diagram	7
1.7	Stellar clusters	7
1.7.1	Open clusters	7
1.7.2	Globular clusters	8
2	Characteristics of the experimental setup	9
2.1	The cooling process	9
2.2	Flat field corrections	11
2.3	Linearity and dynamical range of the CCD	11
3	Globular Cluster BS90¹⁴	13
3.1	Zeropoint calibration	13
3.2	PSF photometry with STARFINDER	14
3.2.1	The basic idea of PSF fitting	15
3.3	Color Magnitude Diagram for BS90 ¹⁴	16
4	Conclusion and final discussion	I
List of Figures		II

1 Fundamental principles of astronomical measurements

Most of the times we are trying to obtain astronomical data we measure electromagnetic radiation.

Unfortunately there are two basic problems with this approach. On the one hand we are dealing with huge distances in space, which lead to very small intensities and on the other hand we can not achieve any kind of laboratory conditions like in space, due to the mere lack of a laboratory which is large enough.

1.1 Detectors in Astronomy

The evolution of detectors in astronomy started simple, with people looking in the sky. Soon scientists realized that it's more precise and reliable to take pictures which ultimately lead to today's standard, charged couple devices (CCD's).

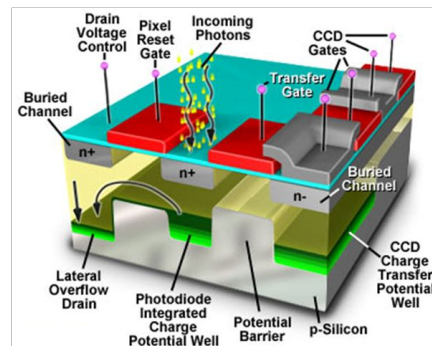
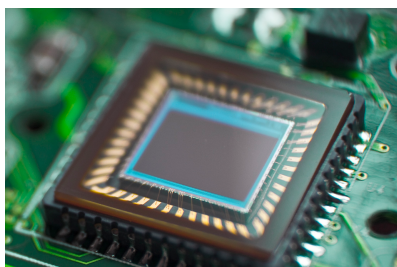


Figure 1.1: Image of a CCD chip and a schematic overview of its functionality.

These are semiconductor detectors, that use the inner photoelectric effect to convert incoming radiation into a separated charge, that can be read out. A CCD consists of a two dimensional grid of light sensitive metal oxide semiconductors, that act as capacitors. Incoming photons excite electrons into the conduction band, after which the electrons are trapped in the capacitors potential wells. At this point they can easily be read out and converted into a digital signal.

This technique had such a big impact on astronomy because of the following fundamental advantages compared to other light detectors:

1. **high sensitivity:** CCDs achieve a quantum efficiency of up to 90%.
2. **high dynamic range:** Dynamic range characterises the "levels of brightness", that can be detected by one device. Therefore a high dynamic range is helpful in astronomy, because we are dealing with stars that are visible with the bare eye, as well as objects we receive single photons from.
3. **linearity over almost the entire dynamic range:** The detector signal is to an amazing degree proportional to the incoming photon flux, up until the detector is saturated. This is a helpful property when comparing objects on the same image as well as on different images. Nevertheless the exposure time should be chosen very carefully, because to make sure to receive a useful signal to noise ratio.
4. **direct availability for further computer-aided data analysis:** Unlike all analogue forms of photography and photometry the data collected by a CCD is immediately converted into a digital signal, without any quality loss or other additional problems.

Of course, as always, there are some drawbacks. For one it has to be considered that some pixels are dead (their output has no meaning). Also, some pixels are activated by cosmic radiation, such as γ -rays, muons and electrons. These pixels or even the area around them mostly appear to be saturated or to have an unlikely high count.

Both these events can be counteracted by taking multiple measurements with slightly different camera angles. The dead pixels will stay at their exact position, while the pixels activated by other kinds of radiation will randomly change place. Therefore it is possible to get rid of both these errors, the described technique is called "dithering" or "jittering".

1.2 Data Reduction

Imperfections in the manufacturing process of CCDs lead to some variations of the sensitivity of each pixel

1.3 Basics of photometry

What we are observing in our measurements is the **radiation flux** F of the stars which is given by

$$F = \frac{L}{4\pi d^2} \quad (1.1)$$

where d is the distance between the observer and the star and L is its luminosity. To normalize our measured values we are using the sun as reference for the units we choose. For example the luminosity of the sun is $1 L_\odot = 3.846 \cdot 10^{26}$ W.

The **Stefan-Boltzmann law** explains the connection between the surface temperature of a star and his flux. It is given by

$$F = \sigma T_{\text{eff}}^4 \quad (1.2)$$

with the Stefan-Boltzmann constant $\sigma = 5.67 \cdot 10^{-8} \text{ W m}^{-2} \text{ K}^{-4}$. To understand the meaning of the effective temperature T_{eff} we need to know what we understand as a **black body**. A black body is, in theory, an object that absorbs every radiation independent on the corresponding wavelength and doesn't reflect any of it. The effective temperature in (1.2) is the temperature a black body with the same surface as the star would need to emit the same radiation power.

We already introduced a new quantity, the luminosity of a star which is defined as the surface area A times the flux. From this we can derive a relation between luminosity and temperature using (1.2):

$$L = 4\pi R^2 \sigma T_{\text{eff}}^4 \quad (1.3)$$

with the radius R of the star.

Another interesting parameter in astronomical observations are the masses of the observed stars, which determine their evolution. In particular the initial mass of the star is the parameter that allows us to predict his fate. But unfortunately the determination of star masses from single measurements is not trivial.

As one can conclude from (1.1), the intensity of the incoming flux of the star, e.g. the number of photons detected decreases with the square of the distance. The problem is that the distance is not directly known for most observations. This and the fact that every instrumental setup is different leads us to the introduction of different magnitude scales to be able to determine luminosities and compare results taken from various observations.

These different scales are explained in the following section.

1.4 Magnitudes

To solve the problem mentioned above we introduce three different magnitude scales and another scale including the wavelength independency of the observed radiation.

1.4.1 Instrumental Magnitude

The instrumental magnitude allows us to compare measurements of different objects within the same measurement or during different sessions at the same instrumental setup under the same conditions.

It is a relative unit, converting the measured counts to a logarithmic scale with an arbitrary zeropoint, e.g.

$$m_{\text{instr.}} = \text{zeropoint} - 2.5 \log_{10}(\text{counts}) \quad (1.4)$$

With the help of so called standard stars whose magnitude is already known and the fitting of a point spread function (PSF), which will be explained in detail later, one can convert the relative instrumental magnitude into the apparent magnitude.

1.4.2 Apparent Magnitude

This magnitude scale takes the earth as reference point and measures the brightness of the star as perceived from its surface, assuming a logarithmic perception of the brightness by the human eye. This scale was already introduced by Hipparch at ~ 150 b.c., then using brightness classes ranging from 1 (brightest stars) to 6 (barely visible). Nowadays a difference of five magnitudes corresponds to a factor of 100. With this scaling one finds the following formula for the flux ratio of two stars:

$$\frac{F_2}{F_1} = 100^{(m_1 - m_2)/5} \quad (1.5)$$

As before standard stars are used to determine the offset between instrumental and apparent magnitude and thereby calibrating the scale. Now we are able to compare different magnitudes obtained from different measurements and with different circumstances.

1.4.3 Absolute Magnitude

Directly resulting from the conceptual idea of the apparent magnitude we finally introduce the absolute magnitude as the apparent magnitude a star would have if they were a distance of 10 pc¹ away.

The distance has been chosen arbitrarily. This allows us to physically compare the absolute brightness of different stars at different distances. One can now calculate the ratio between the actual measured flux (the apparent magnitude m) and the hypothetical magnitude of the flux if the star was actually 10 pc away.

$$\frac{F(10 \text{ pc})}{F} = \left(\frac{d}{10 \text{ pc}} \right)^2 = 100^{(m - M)/5} \quad (1.6)$$

In this formula, m represents the apparent magnitude and M the absolute magnitude. Now we are able to compute the absolute brightness of every star, if we know its distance d and the corresponding apparent magnitude. If the distance is, as usually, not known and other methods lead to a determination of the stars absolute brightness, we are able to use the following formula to find the distance of the observed star:

$$d = 10^{(m - M + 5)/5} \text{ [pc]} \quad (1.7)$$

where the expression $m - M = 5 \log_{10} d[\text{pc}] - 5$ is called the distance modulus.

If two stars are located at the same difference from the observer the following relation holds:

$$\frac{F_2}{F_1} = \frac{L_2}{L_1} = 100^{(M_1 - M_2)/5} \quad (1.8)$$

As a result, for known luminosity and absolute magnitude of a reference star we can determine the luminosity of any other star at the same distance from its absolute magnitude.

¹The distance 1 pc = 3.263 ly = $3.086 \cdot 10^{16}$ m.

1.5 Bolometric Magnitude

We distinguish wavelength-dependent and bolometric magnitudes, which are integrated over the total wavelength range.

Due to limitations in the respective spectral range of the detectors it is often hard to determine the bolometric amplitude M_{bol} . We want our measurements to be as precise as possible. That's the reason why they need to be performed by space observatories to avoid absorption processes due to the earth's atmosphere.

If one nevertheless wants to estimate the bolometric magnitude from measurements from earth, we need to introduce wavelength-dependent magnitudes M_{λ} which cover only one part of the total spectral range.

To realize this, we can use different well-defined filters, which let us concentrate our measurements on specific ranges.

In the following table one of the most commonly used filter systems, the Johnson system is presented. Here λ_0 describes the respective central wavelength and $\delta\lambda$ the corresponding spectral width.

Filter	λ_0 [nm]	$\delta\lambda$ [nm]	spectral range
U	365	66	ultraviolet
B	445	94	blue
V	551	88	visual (green)
R	658	138	red
I	798	-	infrared

Table 1.1: The spectral setup of the Johnson filter system [2]

By measuring different filter constellation one can compute a distance-independent color index

$$m_B - m_V = M_B - M_V = B - V \quad (1.9)$$

which gives us information on the spectral properties of the object.

To correct any fractional deviations from a perfect filter system the following correction formula, including the apparent magnitude B in the Johnson system and the measured instrumental magnitude b is presented:

$$B = b + b_0 + c_B(b - v) + a_b \cdot \text{airmass} \quad (1.10)$$

The other correction terms have to be computed again by comparison with standard stars. The assumption made to obtain this formula was a slightly different transmission curve for the B filter.

1.6 The Hertzsprung-Russel-Diagram

After having classified enough stars through observation, astronomers were able to perform statistical analysis.

It was noticed, that the spectral classification of the stars was related to some basic parameters such as mass or luminosity. For example the so called *O* stars which are located at the end of the classification scheme were observed to be young, massive and luminous whereas the *M* stars on the other side of the scheme have a low mass and are barely visible.

This fundamental relation between the spectral type of a star, which is physically connected to his effective temperature T_{eff} , and his luminosity can be visualized in a **Hertzsprung-Russel-Diagram** (HRD).

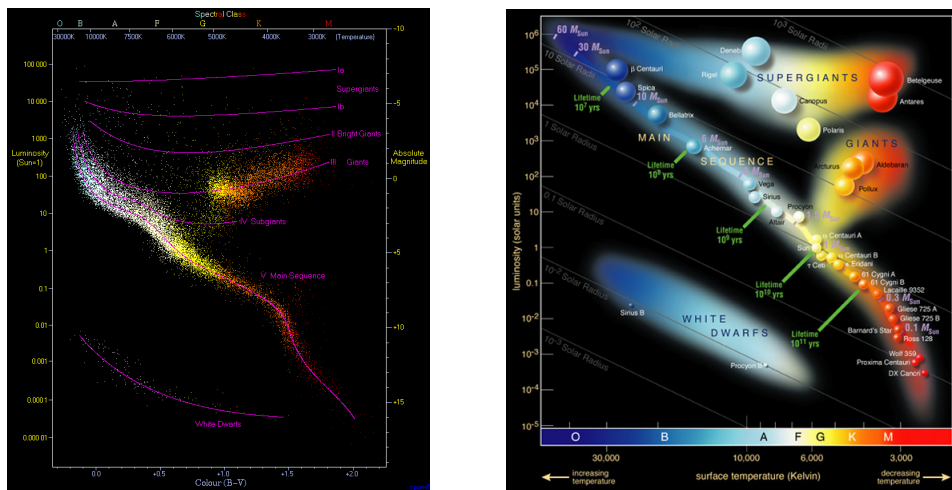


Figure 1.2: An observational HRD with 22.000 plotted stars from the Hipparcos catalogue and a schematic picture of a HRD showing some well-known stars in the milky way

One can easily see, that most stars are located near the so called main sequence, which is characterized by the hydrogen burning phase during the main phase of a star's life. In the other regions in the diagram we can find stars in different stages of their life.

As a conclusion one can remark that the HRD shows the evolutionary history of the population.

It's always hard to compute a HRD because as we have already mentioned above the absolute magnitudes or luminosities are often not accessible. The same holds for the determination of the respective spectral classes.

Instead, astronomers use **Color-Magnitude-Diagrams** to visualize the evolution of star clusters. Here, the apparent magnitude V is plotted over the color index $B - V$ which is related to T_{eff} .

To obtain the color index, measurements with at least two filters are needed.

In the following we want to discuss how one can access the relevant data such as the

distance, the age, or the metallicity of the population from the CMD.

1.6.1 Analysis of a Color Magnitude Diagram

First of all we assume that all stars of a cluster are approximately at the same distance, have the same chemical composition and the same age.

By plotting V versus $B - V$ and comparing the position of the main sequence of the cluster with a known cluster, the distance can be estimated. In this approximation we neglect small effects due to varying metallicities.

The shift that is needed to align the main sequence with the one from the known cluster is proportional to the distance modulus of the cluster.

Alternatively one can always compare the CMD with theoretical models for stellar evolutions which are nowadays broadly known.

What we are doing in our evaluation of the cluster is applying a fitting routine to find the positions of the so called **isochrones**, e.g. the curves representing the position of the stars of the same age inside the population.

Another assumption, that all stars of the population were formed approximately at the same time, gives us the possibility to determine the age of the cluster from the CMD.

To understand how this is possible, one needs to understand how the luminosity of stars is dependent on their mass:

$$L \sim M^a \quad (1.11)$$

The exponent a has a mass dependence itself (Here: $a = 3.5$ for $2M_{\odot} < M < 20M_{\odot}$).

One can conclude, that the massive stars on the top left end of the CMD drift to the red giant branch after all their hydrogen has been burned. The older stars with lower masses also start at some time to move into the red giant branch.

The time a star spends on the main sequence is proportional to the ratio $\frac{M}{L}$, e.g.

$$\tau_{\text{nuc}} \sim \frac{M}{L} = M^{(1-a)} \quad (1.12)$$

The shifting points in the sequence are called the **turn-off points**. From the position of the turn-off point one can estimate the age of the cluster. This method leads to good results, especially for older populations. In our fits later in the evaluation part we also vary the metallicity to obtain the best possible fit curve.

1.7 Stellar clusters

This section mainly deals with the classification and the comparison of the two main groups of stellar clusters: Open clusters and globular clusters (GC).

1.7.1 Open clusters

An open cluster is a group of up to a few thousand stars that have roughly the same age. More than 1000 open clusters have been discovered within the Milky Way Galaxy and

many more are thought to exist.

They are weakly bound by gravitational attraction and become disrupted by close encounters with other clusters and clouds of gas as they orbit the galactic center.

Their lifetime is estimated from a few hundred million years up to a few billion years for the most massive ones.

The metallicity of stars in an open cluster varies a lot, depending on age and location within the host galaxy. Normally they are distributed in the disc of the galaxy.

1.7.2 Globular clusters

In this experiment we are dealing with globular clusters, which are in general much older and more massive than the open clusters. They are among the oldest objects in the universe. Other characteristics are that the stars in a GC have a poor metallicity because they consist almost only of hydrogen and helium. This can be explained by the fact, that these were the elements found directly after the big bang. This indicates that the GC must have been formed in the early universe.

They are spherically symmetric and located in the halo of a galaxy. For the Milky Way, around 150 GCs are known. Because they were formed at the early phase of the galaxy's formation they are good references to study their evolution. In general we can conclude that stellar clusters are well-suited for analysis with HRDs or CMDs because the respective diagrams have characteristic forms and therefore it is relatively easy to locate the stars within the diagrams.

2 Characteristics of the experimental setup

In this part we describe how we prepared the telescope and the detector system to be able to take images with a good quality and resolution.

More precisely, we are describing the cooling process, determining the band gap of our detector and we perform flat-field corrections. After that we discuss further details of the properties of the CCD chip which is located inside the detector.

2.1 The cooling process

Before we were able to start with our measurements we had to prepare the telescope by cooling it down with liquid nitrogen to prevent disturbing effects such as thermal activation of electrons that could effect our measurements. First of all we evacuated the cryostat to protect the chip of damage cause by freeze out. This process took about three hours. Using a Python script, we took test images every thirty seconds to obtain the current temperature and to be able to see the effects of the cooling process to the quality of the images. To demonstrate the impact on the resolution of the exposures we present two images, one taken at the beginning of the cooling process with a temperature of $T_{\text{in}} = -4.7 \text{ }^{\circ}\text{C}$ and the other at the end, after reaching the final temperature $T_{\text{f}} = -90.3 \text{ }^{\circ}\text{C}$.

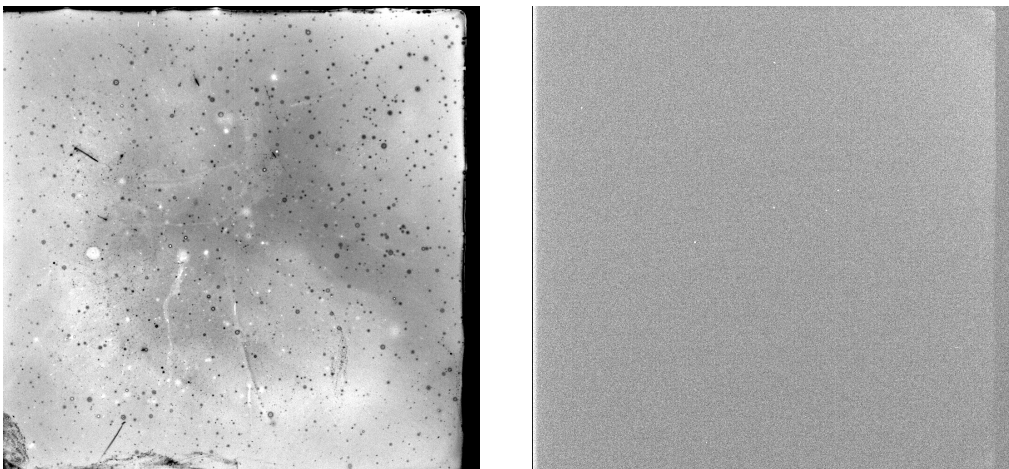


Figure 2.1: Visualization of the impact if the cooling process on the quality of the images.
On the left we see the picture taken at $T = T_{\text{in}}$ on the right at $T = T_{\text{f}}$.

As one can easily see, the quality of the image improved a lot compared to the beginning of the measurement. The structure of the image is now almost homogeneous and we re-

duced nearly all of the disturbing noise. In addition one can already see some of the dead pixels as small white parts which don't contribute to the measurement.

With the temperature data we were able to determine the band gap E_g of the semiconductor by fitting the theoretical curve which describes the dependency of the dark current I from the temperature T using Fermi statistics:

$$I = c_0 \cdot T^{\frac{3}{2}} \cdot \exp\left(-\frac{E_g}{2k_B T}\right) \quad (2.1)$$

The Boltzmann constant k_B is given by $k_B = 8.617 \cdot 10^{-5} \text{ eV/K}$. The result of our measurement is presented in the following diagram.

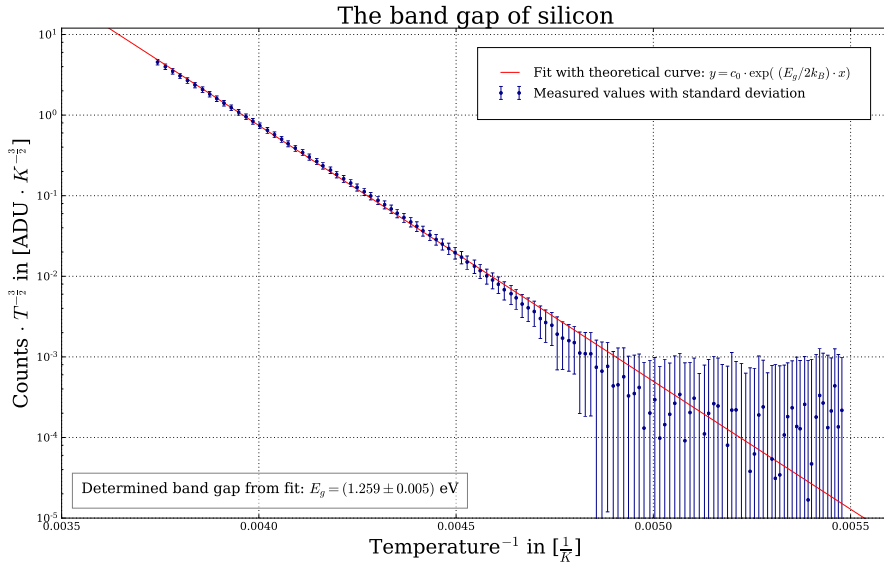


Figure 2.2: Determination of the band gap of silicon as an important characteristic of the experimental setup.

As a result of the measurement we determined the band gap for our detector to:

$$E_g = (1.259 \pm 0.005) \text{ eV} \quad (2.2)$$

The theoretical value for silicon is $E_{g,SI} = 1.15 \text{ eV}$ and therefore slightly smaller than the value we extracted from our temperature measurement.

2.2 Flat field corrections

2.3 Linearity and dynamical range of the CCD

This part of the experiment deals with the limitations of the chip concerning sensitivity to incoming photons, linearity and its dynamical range.

We measured with two different filter constellations, namely the same as in the section before (R- and I-filter).

By plotting the median of the signal against the adjusted integration time for both flat-field images we want to determine the linear regime of the electronics.

The result of the linear fit can be found in the following figure and is discussed after.

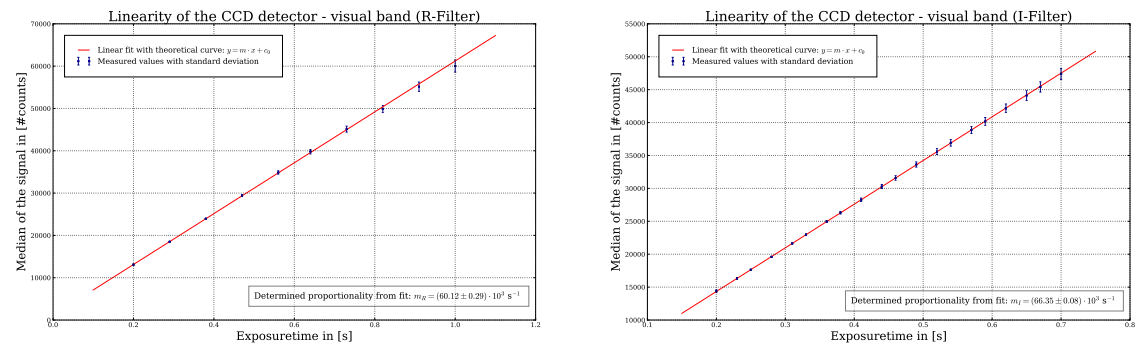


Figure 2.3: Results of the determination of the linear regime of the experimental setup with different filter constellations.

Unfortunately we didn't choose larger integration times to find the domain where the chip is saturated. Therefore we can only conclude which domains are definitely in the linear regime.

Nevertheless we got the following results:

Filter	Counts _{min}	Counts _{max}	gain [counts/s]
R	~ 13000	~ 60000	(60.12 ± 0.29) · 10 ³ s ⁻¹
I	~ 14000	~ 48000	(66.35 ± 0.08) · 10 ³ s ⁻¹

Table 2.1: Determination of the linear regime of the measuring electronics for both filter constellations.

Now we want to investigate the deviation from a perfectly linear relationship by computing the R^2 value for both fits. The R^2 value is a statistical measure of how close the data are to the fitted regression line.

The formal definition is:

$$R^2 = \frac{\sum (\hat{y}_i - \bar{y})^2}{\sum (y_i - \bar{y})^2} = 1 - \frac{\sum (y_i - \hat{y}_i)^2}{\sum (y_i - \bar{y})^2} \quad (2.3)$$

where \hat{y}_i are the values predicted by the linear fit and $\bar{y} = \frac{1}{n} \sum_i y_i$ is the mean of the measured values.

In our case we got the following results:

Filter	R^2 value
R	0.999567242841
I	0.999985446198

Table 2.2: Corresponding R^2 values for our linear fits.

This means our results show a pretty much perfect linear relationship as we expected.

3 Globular Cluster BS90¹⁴

In this part of the experiment we are analyzing the properties of the globular cluster BS90¹⁴. Unfortunately the bad weather conditions during our measurement prevented us from collecting data by ourselves. Instead we are working with images taken by the Hubble Space Telescope (HST).

The goal of this part is to perform PSF fitting for two different filter constellations, matching both images together and finally plot a Color Magnitude Diagram (CMD) to determine age and metallicity of the cluster after fitting different isochrones by varying both parameters.

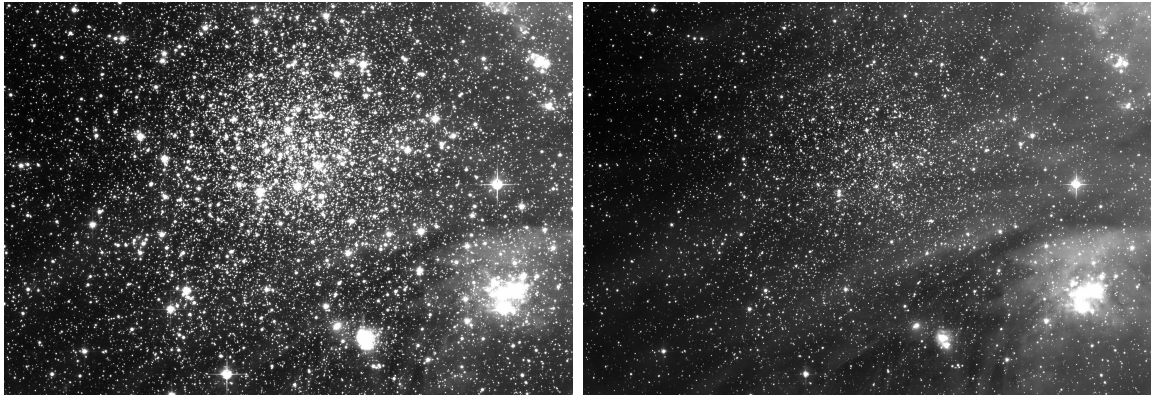


Figure 3.1: Exposures of the globular cluster BS90¹⁴ taken by the Hubble Space Telescope. The image on the left was taken using an I-filter (infrared spectrum), the one on the right using a V-filter (visible spectrum).

3.1 Zeropoint calibration

To calibrate the measured data to a standard scale, which is in this case the apparent magnitude scale, we are comparing the counts of several standard stars with reference values from SIMBAD, an astronomical data base. From these results we can determine the zeropoint p_0 using equation (1.4):

$$p_0 = m_{\text{CATALOG}} + 2.5 \log_{10}(\text{counts})$$

We choose ten suitable stars, e.g. stars that are clearly isolated and bright enough but not yet saturated.

The results of our measurement are enlisted in the following tables .

Star	Mag _V	# _V	$\Delta\#_V$	$p_{0,V}$	$\Delta p_{0,V}$	Mag _I	# _I	$\Delta\#_I$	$p_{0,I}$	$\Delta p_{0,I}$
1	17.78	908	30	25.175	0.036	16.65	1881	43	24.836	0.025
2	17.77	1371	37	25.613	0.029	16.21	4274	65	25.287	0.017
3	17.67	1345	37	25.492	0.030	16.81	3994	63	25.814	0.017
4	17.50	1052	32	25.055	0.033	16.64	2281	48	25.035	0.023
5	17.24	1511	39	25.188	0.028	15.79	4605	68	24.948	0.016
6	18.45	808	28	25.719	0.038	17.10	1738	42	25.200	0.026
7	18.23	885	30	25.597	0.037	16.23	2073	46	24.521	0.024
8	18.09	790	28	25.334	0.038	16.93	1626	40	24.958	0.027
9	17.97	961	31	25.427	0.035	16.68	1837	43	24.840	0.025
10	17.74	764	28	24.948	0.040	16.85	1694	41	24.922	0.026

Table 3.1: Zeropoint calibration by comparing ten stars with SIMBAD references. The left part corresponds to the exposure analyzed with the V -filter, the right part to the one analyzed with the I -filter.

Remark: Due to the limited space we abbreviated counts with #.

We take the mean of the calculated zeropoints p_0 and computed the standard deviation as statistical error and the error propagation as usual to get an estimate of the systematic error.

The final results are the following:

Filter	zeropoint p_0	Δp_0 (syst.)	Δp_0 (stat.)
V	25.334	0.004	0.011
I	24.953	0.004	0.007

Table 3.2: Results of the zeropoint calibration.

3.2 PSF photometry with STARFINDER

We are using STARFINDER to perform statistical PSF fitting, e.g. the IDL takes the positions of about 10 to 30 isolated, unsaturated stars and applies several corrections (subtraction of the background, deblending, etc.).

tion of an average background and normalization of the peak intensities) to both images. Now the software is able to compare the results for all the stars we chose and to determine the final result: an average PSF for the entire image.

3.2.1 The basic idea of PSF fitting

The point spread function (PSF) describes the response of an imaging system to a point source or point object which are in our case the stars on the exposures. The degree of blurring of the point object is a measure for the quality of the image. An important characteristic is that the imaging of two different objects is independent of each other. This is due to the non-interacting property of photons. The image of a complex object can then be seen as a convolution of the true object and the PSF.

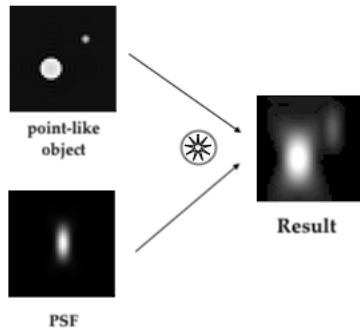


Figure 3.2: Visualization of the key idea of PSF fitting

The radiated field is related to its corresponding source plane distribution via Fourier transform. This is how the algorithm is able to determine the PSF from our exposures.

Applying this idea to our problem:

We chose about 25 stars and selected the most suitable, e.g. those who were as centered and symmetric as possible for the fitting.

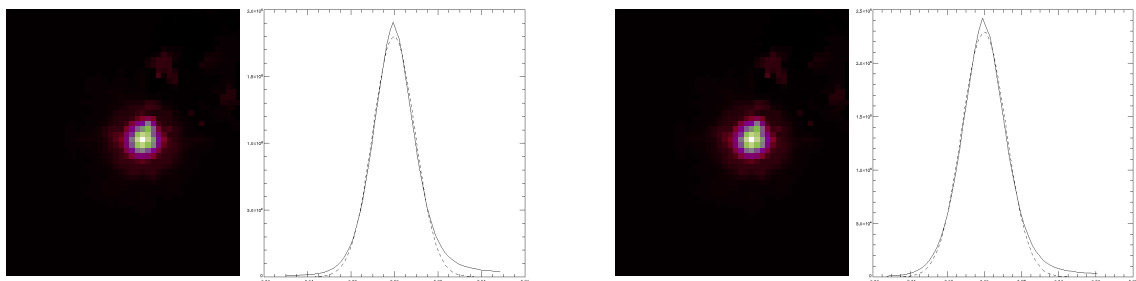


Figure 3.3: Results of the PSF fit for the I-filter (left) and the V-filter (right).

With these results STARFINDER is able to detect all potential stars by dividing the image into smaller parts and checking if the analyzed objects are brighter than the estimated threshold. Using this technique the program is only able to determine the instrumental magnitude if the sources. The result from the zeropoint calibration performed in (3.1) becomes important now to get the corresponding apparent magnitudes. After finishing the iteration for both images we get a list of all stars which could be detected.

To finally obtain the CMD for our cluster we need to match the stars found in both pictures. This cross matching process is done with the help of the Python script `matchstars.py` located on our working computer at MPIA.

3.3 Color Magnitude Diagram for BS90¹⁴

We are now able to plot the CMD (V versus V-I) and fit matching theoretical isochrones by varying different parameters in the script used for plotting (`cmdplot.py` also available on the working computer) such as the **shift** of the image, the **metallicity** or the **age** of the cluster.

The resulting Color-Magnitude diagram is presented in figure (3.4):

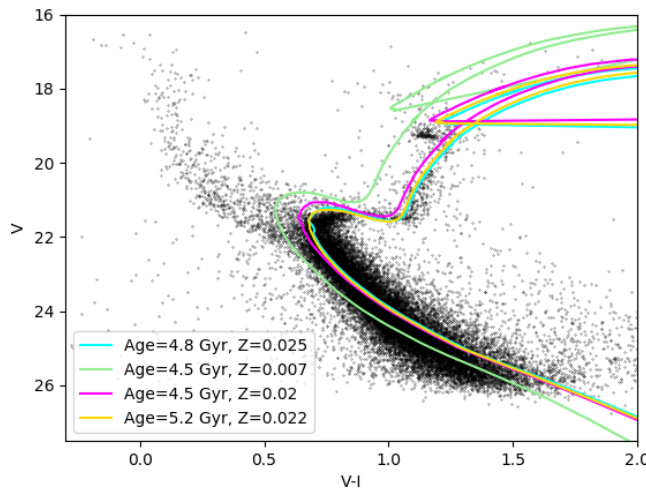


Figure 3.4: Color-Magnitude diagram with theoretical isochrones for BS90¹⁴

We fitted a total of four possible isochrones with different parameters. The quality of our results is discussed subsequently.

Isochrone [color]	Age [Gyr]	Metallicity Z
blue	4.8	0.025
green	4.5	0.007
magenta	4.5	0.020
yellow	5.2	0.022

Table 3.3: Fitting of the theoretical isochrones in our CMD.

The green isochrone doesn't seem to be a good reference, because one can clearly see that there is a large deviation between the curve and structure of the cluster.

We included it only due to the fact that the parameters chosen for this case match with the literature values.¹

For all of the other curves we tried to find the best possible combination of parameters. Nevertheless we recognize a significant difference between the values for the metallicities we found and the value from the paper. Possible reasons for this deviation are discussed in the conclusion.

¹Reference values can be found in this paper: <https://arxiv.org/pdf/0704.2942.pdf>

4 Conclusion and final discussion

References

- [1] Pierre Léna. *Observational Astrophysics*. 3. Auflage. Berlin ; Heidelberg: Springer, 2012.
- [2] Jörg-Uwe Pott. *FP 30: CCD photometry in modern astronomy - manuel*. Version 4.0.3. MPI for Astronomy, Heidelberg, 2017.
- [3] Albrecht Unsöld and Bodo Baschek. *Der neue Kosmos. Einführung in die Astronomie und Astrophysik*. 7. ed. Berlin ; Heidelberg: Springer Spektrum, 2015.

List of Figures

1.1	Image of a CCD chip and a schematic overview of it's functionality.	1
1.2	An observational HRD with 22.000 plotted stars from the Hipparcos catalogue and a schematic picture of a HRD showing some well-known stars in the milky way	6
2.1	Visualization of the impact if the cooling process on the quality of the images. On the left we see the picture taken at $T = T_{\text{in}}$ on the right at $T = T_{\text{f}}$	9
2.2	Determination of the band gap of silicon as an important characteristic of the experimental setup.	10
2.3	Results of the determination of the linear regime of the experimental setup with different filter constellations.	11
3.1	Exposures of the globular cluster BS90 ¹⁴ taken by the Hubble Space Telescope. The image on the left was taken using an I-filter (infrared spectrum), the one on the right using a V-filter (visible spectrum).	13
3.2	Visualization of the key idea if PSF fitting	15
3.3	Results of the PSF fit for the I-filter (left) and the V-filter(right).	15
3.4	Color-Magnitude diagram with theoretical isochrones for BS90 ¹⁴	16